Pergamon

Int. J. Solids Structures Vol. 33, No. 25, pp. 3673–3696, 1996

0020–7683/96 $15.00 + .00

0020-7683(95)00209-X

STRESS DISTRIBUTION AND CRACK INITIATION FOR AN ELASTIC CONTACT INCLUDING FRICTION

MATS ANDERSSON
Royal Institute of Technology, Department of Solid Mechanics, S-100 44 Stockholm, Sweden

(*Received* 23 *February* 1995; *in revised form* 23 *August* 1995)

Abstract—In a contact between a spherical indenter and the plane surface of a brittle solid, experimental studies show that circular cracks emanate outside the edge of the contact region, not at the contact edge as expected from the Hertz solution.

In this paper different levels of approximation where friction is accounted for, are compared with the solution of the fully coupled contact problem. In particular, the maximum tensile principal stress and its location are computed. The location of the calculated maximum stress is compared with the radius of the ring crack found in indentation tests. It is shown that an uncoupled analysis with a stick and a slip zone gives accurate results for most practical material combinations.

The coefficient of friction is experimentally measured by use of a leaning plane. Comparisons are made with experiments performed on ceramics and glass, which show that the use of the measured coefficients of friction will predict a smaller crack initiation radius than those found from experiments. Copyright © 1996 Elsevier Science Ltd

1. INTRODUCTION

In recent years the use of indentation tests on brittle materials has grown in popularity as a method for the determination of material properties such as Young's modulus, tensile strength, fracture toughness and of course hardness (Zeng *et al.*, 1992a,b). Several well known test methods, like Vickers, Rockwell, Knoop, Berkovich (for nano-indentation) and Brinell are used. A major advantage of indentation tests is the relative ease of how to perform them, while a drawback is that the indenters inevitably give rise to complex stress fields. To evaluate these tests the details of the stress distribution of the bodies have to be known. This is advantageous for the Brinell test since the problem of a sphere indenting a half-space, at least for linear elastic behaviour, has a closed form solution. The drawback of the Brinell test, as compared to the other tests is that the solution is not self similar which complicates the analysis for inelastic material behaviour.

The problem of elastic contact between two solids is usually treated in a way where the indentation is assumed to take place without influence of friction, allowing for shear free sliding. The mathematical solution to this problem for a smooth contact was found by Hertz over hundred years ago and is well known. For this case the maximum principal tensile stress is the radial stress at the contact perimeter. In brittle materials, discarding statistical effects, the first cracking should therefore be initiated at this point.

Experiments show, however, that the first crack (circular) usually has a radius 5–40% larger than the contact radius. It is the author's opinion that this, to a great extent, is due to the presence of friction which changes the stress distribution and therefore shifts the location of the largest principal stress. There are, however, other explanations for the divergence, for example statistical effects from presence of surface flaws, their size distribution, and thus energy release rate (Lawn and Wilshaw, 1975 and Mouginot and Maugis, 1985). The flaw size explanation is supported by the fact that polishing the surface, and thereby removing the flaws, results in a crack radius that is closer to the contact radius (Chaudri and Phillips, 1990). Polishing will also decrease the coefficient of friction, indicating that the result also supports the hypothesis that friction is of major importance. A point frequently missed when using statistical models for the largest flaw size is the repetitive nature of the experimental results. The shape of the ring cracks are, for isotropic materials

also, indeed very circular. Both these two observations indicate that the crack pattern is determined by the stress distribution primarily. Also the influence of surface roughness has been suggested as an explanation (Greenwood and Tripp, 1967). However, brittle materials like ceramics and glasses usually have smooth surfaces and the contact pressure is high when cracking occurs. Under such circumstances the influence of surface roughness on the contact pressure distribution is negligible. A problem with the definition of the contact radius in this analysis also persists, which complicates the use of this type of analysis. Also the predicted increase of contact radius has not been observed in experiments.

In Johnson *et al.* (1973), in a thorough study, different theories for crack initiation are compared with experiments on glass. Here, it is pointed out that friction qualitatively gives a correct explanation of the fact that cracks occur outside the contact as well as that cracks occur during unloading (reverse slip occurs increasing the tensile stress). However, the approximate calculation of the stress fields does not give quantitative agreement.

The contact problem including friction has been solved by Spence (1975) using a combined analytical and numerical method. It requires the solution of two coupled integral equations of Fredholm's first kind. This is complicated, and if the stress distribution is sought, integration of both normal and shear stress distributions has to be performed. There are also several solutions found by use of FEM or BEM. In these numerical methods it is quite difficult to capture the large gradients of the solution around the contact edge even without any frictional forces. In particular, the radial stress at the surface is practically impossible to calculate accurately. To perform a parameter study with reasonable accuracy would therefore require massive amounts of computer time.

The influence of friction was widely studied in the sixties and at the beginning of the seventies (Goodman, 1962, Spence, 1968, 1973, 1975, Noble and Spence 1971 and Johnson *et al.*, 1973). Contact stresses were computed and compared for different levels of approximation. It was also shown that the presence of friction radically changes the stress distribution in the contact region. What has not been performed is a systematic study of the accuracy of the stress distributions calculated from the uncoupled analysis. This is of particular interest when the dissimilarity between the bodies is significant.

In this paper a parametric study is performed for the fully coupled problem as well as for three different types of uncoupled analysis. The change in radial stress is primarily studied. The contact pressure and shear stress distribution will depend upon the coefficient of friction μ and the level of dissimilarity of stiffness for the contacting materials β. The stress distribution will also depend of Poisson's ratio ν. In order to find reliable values of the coefficient of friction, measurements for different material combinations have been performed. Finally the calculated location of the maximum stress is compared with the radius of ring cracks found in indentation experiments.

2. SOLUTION TECHNIQUES

Consider a contact between a sphere and a half-space according to Fig. 1. A basic assumption is that Coulombs law of friction is valid point wise, e.g.

$$q(x) \leqslant \mu p(x), \tag{1}$$

where μ is the coefficient of friction which is assumed constant. It does not depend either upon the spatial coordinate x (which will be valid if the surfaces are uniform), or the pressure p. Experience has shown the latter to be true, at least for a wide range in pressure magnitude.

Depending on the required accuracy different levels of approximation can be adopted. The exact solution requires the solution of two coupled integral equations. The solution has to be found numerically and therefore also stresses are found by numerical integration. If, on the other hand, the influence of friction on the normal pressure is neglected, the problem becomes uncoupled. The resulting integral equation can be solved and thereafter the stresses can be evaluated. The functions involved are quite complicated and some numerical calculations also have to be performed. A further simplification is to assume that

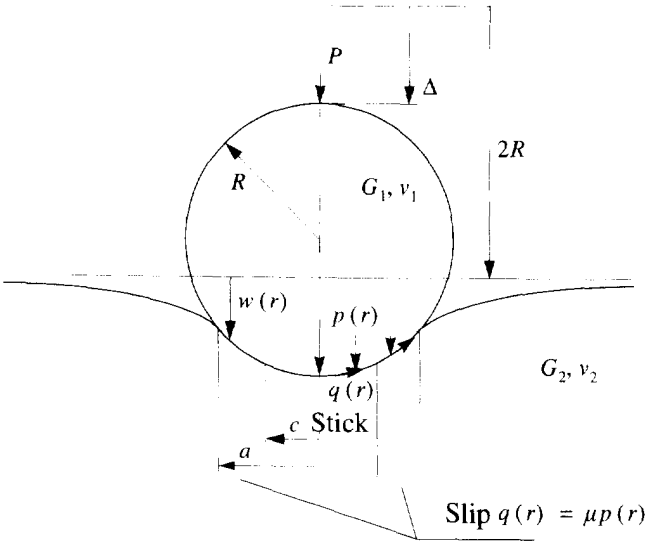

Fig. 1. Definition of geometry and variables used.

either slip or stick occur over the entire contact region. All these cases has been considered and the results will be compared in the following.

2.1. *Coupled analysis*

This problem was first solved by Goodman (1962) using an incremental technique. Later, Spence (1968) used similarity arguments which simplified the analysis. A condensed version of the analysis in Spence (1975) is given here mainly to show the technique and incorporate some improvements. Consider an axisymmetric contact problem. In cylindrical coordinates the stresses and displacements at the surface are written in non-dimensional form as

$$\sigma_{zz}(r) = -\frac{E_c\Delta}{2a}p(x), \quad \sigma_{rz}(r) = -\frac{E_c\Delta}{2a}q(x), \tag{2}$$

$$u_z(r) = \Delta(P)w(x), \quad u_r(r) = \Delta(P)u(x), \tag{3}$$

where

$$\frac{1}{E_c} = \frac{1-\nu_1}{2G_1} + \frac{1-\nu_2}{2G_2}, \tag{4}$$

$x = r/a$, G is the shear modulus, ν is Poisson's ratio, Δ is the indentation depth and a is the contact radius. The subscripts 1 and 2 refer to material (or body) 1 and 2, respectively. If the two bodies in contact are considered to be much larger than the contact radius, the functions p, q, u and w are connected by the pair of coupled Volterra equations

$$\int_x^1 \frac{tp(t)\,dt}{\sqrt{t^2-x^2}} - \beta\left\{\int_0^1 q(t)\,dt - x\int_0^x \frac{q(t)\,dt}{\sqrt{x^2-t^2}}\right\} = \hat{w}(x), \tag{5a}$$

$$x\int_x^1 \frac{q(t)\,dt}{\sqrt{t^2-x^2}} - \beta\int_0^x \frac{tp(t)\,dt}{\sqrt{x^2-t^2}} = \hat{u}(x) \tag{5b}$$

where β is one of the Dundurs' parameters defined as

$$\beta = \left(\frac{1-2\nu_1}{2G_1} - \frac{1-2\nu_2}{2G_2}\right) \Big/ \left(\frac{1-\nu_1}{G_1} + \frac{1-\nu_2}{G_2}\right). \tag{6}$$

The Volterra equations can be written in terms of a single linear integral operator, with a matrix structure as

$$L\begin{bmatrix} p \\ q \end{bmatrix} = \begin{bmatrix} \hat{w} \\ \hat{u} \end{bmatrix}. \tag{7}$$

The simplest way to obtain the solution to the problem of a spherical indenter is to first solve the problem of a flat punch indenting the half-space and then transform the solution to the sphere case. For the flat punch the dimensionless normal displacement has the following form

$$w(x) = 1, \quad 0 \leqslant x \leqslant 1. \tag{8}$$

Within the annulus where no relative slip occurs ($0 \leqslant x \leqslant c$) the following relation holds

$$u = 0, \quad \mu p(x) - q(x) > 0. \tag{9}$$

The corresponding relation in the slip region ($c \leqslant x \leqslant 1$) is

$$u < 0, \quad \mu p(x) - q(x) = 0. \tag{10}$$

Thus, eqn (7) becomes

$$L\begin{bmatrix} p \\ q \end{bmatrix} = \begin{bmatrix} 1 \\ 0, \hat{u} \end{bmatrix}. \tag{11}$$

For a spherical indenter of radius R, the dimensionless normal displacement is

$$w(x) = 1 - \frac{a^2 x^2}{2R\Delta}, \quad 0 \leqslant x \leqslant 1. \tag{12}$$

For a self similar solution to exist, w must be independent of a, thus

$$\Delta = A\frac{a^2}{R}, \tag{13}$$

where A is a constant. With the requirement that there should be no relative slip for $x \leqslant c$ and independence of a, the dimensionless radial displacement must of similarity reasons be of the form

$$u(x) = Cx^2, \quad 0 \leqslant x \leqslant 1, \tag{14}$$

where C is a constant. Thus, for the sphere problem, eqn (7) becomes

$$L\begin{bmatrix} p \\ q \end{bmatrix} = \begin{bmatrix} 1 - x^2/2A \\ 3\pi C x^2/4, \hat{u} \end{bmatrix} \tag{15}$$

The constants A and C have to be determined as part of the solution, with aid of the further boundary condition that the stresses at the edge of the contact region must vanish, i.e.

$$p(1) = q(1) = 0. \tag{16}$$

Since the solution has to be found in an iterative manner, it is more efficient to instead solve the punch problem and then transform the results to the sphere problem (this can be done for any indenter of power law type). If the solution found for the punch is denoted with p_0, q_0 Spence (1968) has shown that the solution for the sphere problem is found as

$$p(x) = 2x\int_x^1 \frac{p_0(t)}{t^2}\,\mathrm{d}t, \quad q(x) = 2x\int_x^1 \frac{q_0(t)}{t^2}\,\mathrm{d}t. \tag{17}$$

The constant A is found from the equation

$$1 - \frac{1}{2A} = \frac{2}{\pi}\int_0^1 tK(t)p(t)\,\mathrm{d}t, \tag{18}$$

where $K(t)$ is the complete elliptic integral of first kind. If the indentation depth is known, the physical contact radius is found by use of eqn (13), giving

$$a = \frac{1}{\sqrt{A}}\sqrt{\Delta R} = \frac{1}{\sqrt{A}}a_H \tag{19}$$

where a_H is the contact radius for the frictionless problem (Hertz solution). Through integration of eqn (2) the relation between the load and the indentation is found as

$$P = 2E_e a\Delta P^* \tag{20}$$

where

$$P^* = \frac{\pi}{2}\int_0^1 xp(x)\,\mathrm{d}x. \tag{21}$$

Thus, in the frictionless case we have $P^* = 1$ for the punch and $P^* = 2/3$ for the sphere. If it is the load that is a priori known (instead of the indentation depth), the physical contact radius is found by combining eqns (13) and (20) as

$$a = \sqrt[3]{\frac{PR}{2E_e AP^*}} = \sqrt[3]{\frac{2}{3AP^*}}a_H. \tag{22}$$

2.2. *Numerical procedures*

For the numerical solution of the integral eqns (11), $p_0(t)$ and $t^{-1}q_0(t)$ are approximated as piecewise constant over N subintervals $h_i = \{t : t_{i-1} < t < t_i\}$ spanning the full interval (0,1). The resulting equations are satisfied at the N midpoints $x_i = (t_{i-1} + t_i)/2$. The slip radius c is chosen as the M^{th} point of subdivision, giving

$$c = t_M, \quad M < N. \tag{23}$$

Since the shear traction in the slip zone can be replaced with the normal pressure times the coefficient of friction, there will be $N + M$ unknowns such that

$$p_0(t) = p_{0i}, \quad \text{for} \quad t \in h_i, \quad i = (1, N) \tag{24}$$

$$t^{-1} q_0(t) = \begin{cases} p_{0i-N}, & i = (1, M) \\ \dfrac{\mu}{x_i} p_{0i}, & i = (M+1, N). \end{cases} \tag{25}$$

Then an equation system is created by insertion of eqns (24) and (25) into (11) giving a system of the type

$$\sum_{l=1}^{M-N} D_{kl} p_l = e_k \tag{26}$$

where the elements of D become

$$D_{ij} = \begin{cases} A_{ij} \\ A_{ij} + \mu\beta\left(\dfrac{x_i}{x_j} B_{ij} - h_j\right) \end{cases} \quad D_{i+N,j} = \begin{cases} -\beta B_{ij} & j = (1, M) \\ -\beta B_{ij} + \mu \dfrac{x_i}{x_j} A_{ij} & j = (M+1, N) \end{cases} \tag{27}$$

$$D_{i,j+N} = \beta(x_i B_{ij} - x_j h_j), \quad D_{i-N,j+N} = x_i A_{ij} \quad j = (1, M)$$

(two minus signs are missing in eqn (2.2) of Spence, 1975) where

$$\left.\begin{matrix} A_{ij} \\ B_{ij} \end{matrix}\right\} = \int_{h_j} \frac{t\,dt}{|t^2 - x^2|^{1/2}} \quad \begin{cases} (t > x_i) \\ (t < x_i) \end{cases} \tag{28}$$

$A_{ij} = 0$ for $j < i$ and $B_{ij} = 0$ for $j > i$. The components of the right hand side are

$$e_k = \begin{cases} 1 & k = (1, N) \\ 0 & k = (N+1, N+M) \end{cases} \tag{29}$$

In order to validate the accuracy of the numerical procedure, comparisons were made with two cases with known analytical solutions, namely the frictionless problem (complete slip) and the adhesive problem (complete stick). With an interval length $h_i = 0.004$ ($N = 250$) the method renders very accurate results. Comparison is done with the frictionless solution where the exact values for the punch are $p_0(0) = 2/\pi \approx 0.636620$ and $P_0^* = 1$. For the adhesive case the solution is dependent upon β and for the maximum value ($\beta = 0.5$) the exact values are $p_0(0) = 0.807860$ and $P_0^* = 1.09861$. As can be seen in Table 1, the agreement is excellent. The pressure distribution also follows the exact solution except for the last two or three points where oscillations occur and the error is quite significant. This behaviour was also reported in Spence (1975). This behaviour may possibly be removed by use of some other functional behaviour of the pressure distribution than piecewise constant. Attempts with a cubic spline distribution used earlier with success (Andersson and Nilsson, 1995) proved worse, giving oscillations over a larger region.

Table 1. Accuracy of the numerical method

	Punch				Sphere				
μ, β	$p_0(0)$	Error (‰)	P^*	Error (%)	$p(0)$	Error (‰)	P^*	Error (‰)	a
$0, \beta$	0.63661	0.02	0.99998	0.02	1.27322	0.01	0.66666	0.01	1.00002
$\infty, 0.1$	0.64196	0.02	1.00333	0.02	1.28394	0.01	0.66889	0.02	0.99861
$\infty, 0.3$	0.68858	0.06	1.03168	0.05	1.37717	0.07	0.68779	0.05	0.98672
$\infty, 0.5$	0.80779	0.25	1.09846	0.14	1.61561	0.26	0.73231	0.13	0.95866

The pressure and shear traction distributions for the sphere were then calculated according to eqn (17). Using the piecewise constant punch pressure p_{0i} the pressure for the sphere becomes

$$p_i = 2x_i \int_{x_i}^{1} t^{-2} p_0(t)\,\mathrm{d}t = 2x_i \sum_{j=i}^{N} p_{0j} \int_{h_j} t^{-2}\,\mathrm{d}t. \tag{30}$$

For the shear traction the corresponding expression is

$$p_{i+N} = \begin{cases} 2x_i \left[\sum_{j=i}^{M} p_{0j-N} \int_{h_j} t^{-1}\,\mathrm{d}t + \mu \sum_{j=i}^{N} p_{0j} \int_{h_j} t^{-2}\,\mathrm{d}t \right] & i = (1, M) \\ \mu p_i & i = (M+1, N) \end{cases}. \tag{31}$$

These integrals were integrated exactly. This is not in accordance with Spence (1975), who performed a quadratic fit on each interval of the flat punch values at the three nearest midpoints before performing the integration. This method was also examined here but proved to be less accurate. After the transformation the same comparison was made as for the punch solution. The solutions are related through eqn (17), which for $x = 0$ gives $p(0) = 2p_0(0)$ and $P^* = 2P_0^*/3$. As can be seen in Table 1 the sphere solution is equally accurate and no additional errors are introduced through the transformation. The oscillations present in the punch solution disappear, and the sphere pressure distribution smoothly approaches zero at the contact radius.

The constant A also has to be calculated (the constant C is not used) in order to determine the actual contact radius. In Spence (1975) this is done by insertion of the sphere solution into the discrete version of eqn (15) and then applying a least square fit. Here A is instead calculated directly from eqn (18), again using the piecewise constant punch pressure distribution. This method proved to be both easier and more accurate. The resulting contact radius is also shown in Table 1.

2.3. *Calculation of stresses*

Begin with inferring a similar scaling as for the stresses in the contact zone, viz

$$\sigma_{ij} = \frac{E_c \Delta}{2a_H} \bar{\sigma}_{ij}. \tag{32}$$

Since comparison will be made with the frictionless solution, the contact radius according to the Hertz solution a_H has been used instead of a. This means, that if the indentation depth is controlled, when calculating the dimensionless stresses in the bodies are produced by a contact pressure of magnitude $\sqrt{A}p(x)$ and a shear stress distribution $\sqrt{A}q(x)$. If instead, the load is controlled, the factor $\sqrt{A}$ multiplying the contact stresses will be replaced by $\sqrt[3]{3AP^*/2}$. The dimensionless coordinates

$$\rho = \frac{r}{a_H} = \frac{x}{\sqrt{A}} \tag{33}$$

are also introduced. There exists several techniques to calculate the stress distribution from surface tractions acting over a disc shaped region. Most of the methods have been developed for analytical applications. In order to avoid numerical evaluation of double (or triple) integrals, an alternative method will be used. The method is based on the radial displacement due to an axisymmetric distribution of normal and shear tractions, as given by Noble and Spence (1971).

$$\frac{G}{1-\nu}u_r(r) = -\frac{1-2\nu}{2(1-\nu)r}\int_0^r sp(s)\,\mathrm{d}s + \int_0^a k_2(r/s)q(s)\,\mathrm{d}s \tag{34}$$

where

$$k_2(r/s) = \begin{cases} \dfrac{2s}{\pi r}[K(r/s) - E(r/s)], & r < s \\ \dfrac{2}{\pi}[K(s/r) - E(s/r)], & r > s \end{cases} . \tag{35}$$

By use of Hooke's law and the definition of strain for axisymmetric deformation, the non-dimensional radial stress is found as

$$\bar{\sigma}_{rr} = \frac{(1-2\nu)\sqrt{A}}{x^2}\int_0^x \eta p(\eta)\,\mathrm{d}\eta - \sqrt{A}p(x) + \frac{4\sqrt{A}}{\pi x}\int_0^x q(\eta)\left[\nu K\left(\frac{\eta}{x}\right) - \left(\frac{\eta^2}{x^2-\eta^2} + \nu\right)E\left(\frac{\eta}{x}\right)\right]\mathrm{d}\eta$$
$$+\frac{4\sqrt{A}}{\pi x^2}\int_x^1 \eta q(\eta)\left[\left(\frac{\eta^2}{\eta^2-x^2} - \nu\right)E\left(\frac{x}{\eta}\right) - (1-\nu)K\left(\frac{x}{\eta}\right)\right]\mathrm{d}\eta, \quad x < 1 \tag{36}$$

$$\bar{\sigma}_{rr} = \frac{2(1-2\nu)\sqrt{A}P^*}{\pi x^2} - \frac{4\sqrt{A}}{\pi x}\int_0^1 q(\eta)\left[\left(\frac{\eta^2}{x^2-\eta^2} + \nu\right)E\left(\frac{\eta}{x}\right) + \nu K\left(\frac{\eta}{x}\right)\right]\mathrm{d}\eta, \quad x \geqslant 1. \tag{37}$$

If the piecewise constant punch pressure distribution is used in connection with the transformation integral, eqn (30), the pressure part of eqn (36) can be integrated exactly. This method, however, proved to be inaccurate since the oscillations in the punch pressure values near the contact edge rather strongly affected the stress distribution. Therefore, a piecewise constant sphere pressure distribution was used. Inserting this into eqn (36), the pressure part becomes

$$\frac{(1-2\nu)\sqrt{A}}{x^2}\int_0^x \eta p(\eta)\,\mathrm{d}\eta - \sqrt{A}p(x) = \frac{\sqrt{A}}{2}\left[\frac{(1-2\nu)D}{x^2} - (1+2\nu)p_k\right] \tag{38}$$

where

$$D = -p_k t_{k-1}^2 + \sum_{j=1}^{k-1} p_j(t_j^2 - t_{j-1}^2) \tag{39}$$

and k is such that $t_{k-1} \leqslant x \leqslant t_k$. Again the comparison with the frictionless solution showed excellent agreement. For $\nu = 0.25$ the error was only 0.04‰ both at the centre of the contact and at the contact edge. Outside the contact the error in the stress distribution will be the same as the error in P^*. The contribution from the shear stress was integrated numerically using a piecewise constant distribution. The shear part of eqn (36) proved to be difficult to integrate numerically. For this reason the method of Green and Collins, described in Barber (1982) is used. The shear stress contribution to the radial stress within the contact disc is according to Hills and Sackfield (1987) (the same expression is obtained by use of the method described in Noble and Spence, 1971)

$$\bar{\sigma}_{rr}^q = \frac{2(1-\nu)}{x^2}\int_0^x \frac{\eta s(\eta)}{\sqrt{x^2-\eta^2}}\mathrm{d}\eta - 2\int_0^x \frac{s'(\eta)}{\sqrt{x^2-\eta^2}}\mathrm{d}\eta \tag{40}$$

where

$$s(\eta) = \frac{2\sqrt{A\eta}}{\pi}\int_{\eta}^{1}\frac{q(x)}{\sqrt{x^2-\eta^2}}\,dx \approx \frac{2\sqrt{A\eta}}{\pi}\sum_{j=k}^{N} q_j \int_{h_j}\frac{dx}{\sqrt{x^2-\eta^2}}. \tag{41}$$

2.4. *Uncoupled analyses*

If the influence of the shear tractions on the normal displacement is neglected, the so-called Goodman approximation is valid for small β. Then, the contact radius and normal pressure will be given by Hertz frictionless solution. This is a widely used approximation that gives the opportunity to find closed form solutions for the stress distribution in the entire half-space (Lundberg and Sjövall, 1958). The scaling introduced above gives the radial stress (see for example Johnson, 1985) at the surface due to the Hertz normal pressure (the frictionless case), as

$$\bar{\sigma}_{rr}^{H} = \begin{cases} \dfrac{4}{\pi}\left[\dfrac{1-2\nu}{3\rho^2}\{1-(1-\rho^2)^{3/2}\}-\sqrt{1-\rho^2}\right], & \rho \leqslant 1 \\ \dfrac{4}{\pi}\dfrac{1-2\nu}{3\rho^2}, & \rho \geqslant 1 \end{cases}. \tag{42}$$

The total stress is then found as the sum of the stresses induced by the normal pressure (eqn (42)) and the friction induced stresses given below.

2.4.1. *Partial slip.* Spence has in a series of articles (1968, 1973 and 1975) treated the problem of partial slip. Primarily for a flat ended punch, but by use of the transformation according to eqn (17), the dimensionless shear traction for the spherical indenter is shown by Hills and Sackfield (1987) to be

$$q(\rho) = \frac{4\mu}{\pi}\left[\sqrt{1-\rho^2}-\rho H(c-\rho)\int_{\rho}^{c}\frac{\psi(t,c)}{t^2\sqrt{1-t^2}}\,dt\right], \quad 0<\rho<1. \tag{43}$$

Here H is the Heaviside step function and c the dimensionless radius of the stick zone. The function ψ is defined as

$$\psi(\rho,c) = \frac{2}{\pi}\left[w\rho\int_{0}^{\pi/2}\frac{d\theta}{(1-(1-\rho^2)\sin^2\theta)\sqrt{1-c'^2\sin^2\theta}} - \frac{cK(c')}{\rho}\left\{\frac{w}{c}-\frac{Q_0(w)}{Q_0(c)}\right\}\right], \quad 0 \leqslant \rho \leqslant c,$$

$$\psi(\rho,c) = 0, \quad c \leqslant \rho \leqslant 1, \tag{44}$$

where

$$w^2 = \frac{c^2-\rho^2}{1-\rho^2},$$

$$c'^2 = 1-c^2,$$

$$Q_0(x) = \tfrac{1}{2}\ln\left(\frac{1+x}{1-x}\right). \tag{45}$$

To evaluate these expressions the radius of the stick zone c has to be known. A natural choice made by Hills and Sackfield is to use the relation derived in Spence (1975)

$$\frac{\mu}{\beta} = \frac{Q_0(c)}{cK(c')} \tag{46}$$

which is valid for $\beta \ll 1$. This also makes it possible to normalize the stresses with respect to β or μ.

In Hills and Sackfield (1987) a closed form solution of the stresses for this shear traction distribution is presented, in which use of the method of Green and Collins (see Barber, 1983 and Green and Zerna, 1968) is made. The shear part of the dimensionless radial stress is given by

$$\bar{\sigma}_{rr}^{q} = \frac{2(1-\nu)}{\rho^2} I - \frac{2}{\rho}\frac{\mathrm{d}I}{\mathrm{d}\rho}. \tag{47}$$

Since it is the maximum stress which occurs outside of the contact that is of primary interest, only the expressions for this region are given here. Unfortunately, the expressions given for I in Hills and Sackfield (1987) and Hills *et al.* (1993) are not correct. Here, instead the following expression has been obtained by use of the same technique. Outside the contact region ($\rho \geqslant 1$)

$$I = \frac{8\beta}{3\pi^2}\left[M\{2\rho^3 - 2\rho^2\nu - c^2\nu\} + \frac{3}{4}\left\{\rho^2 \arcsin\frac{c}{\rho} - c\nu\right\}\right.$$
$$\left. + \frac{3}{2}\int_0^c \frac{t(1-t^2)}{\sqrt{\rho^2-t^2}} Q_0(t)\,\mathrm{d}t - \frac{3Q_0(c)}{cK(c')}\int_c^1 \frac{t^2\{K(t')-E(t')\}}{\sqrt{\rho^2-t^2}}\,\mathrm{d}t\right] \tag{48}$$

and from Hills and Sackfield (1987) or Hills *et al.* (1993)

$$\frac{\mathrm{d}I}{\mathrm{d}\rho} = \frac{8}{\pi^2}\left[\beta\left\{M\left(2\rho^2 - \frac{\rho^3}{\nu} - \nu\rho\right) - \frac{c}{3\rho\nu} - \frac{Q_0(c)}{6}\left(\frac{\rho}{\nu}(3-c^2-2\rho^2) - 4\rho\nu\right)\right.\right.$$
$$\left.\left. - \frac{\rho c}{6\nu} - q\rho Q_0\left(\frac{cq}{\nu}\right) - \frac{cq^2}{3\rho\nu}\right\} + \mu\rho\left\{\frac{c}{\nu}\{K(c')-E(c')\} + \int_c^1 \frac{K(t')-2E(t')}{\sqrt{\rho^2-t^2}}\,\mathrm{d}t\right\}\right] \tag{49}$$

where

$$M = \left[\frac{1+c^2}{2} - \frac{E(c')}{K(c')}\right]\frac{Q_0(c)}{c^2} - \frac{1}{2c},$$
$$\nu^2 = \rho^2 - c^2,$$
$$q^2 = \rho^2 - 1,$$
$$t'^2 = 1 - t^2. \tag{50}$$

2.4.2. *Complete stick.* If it is further assumed that the contact is adhesive, the resulting integral equation can be simplified. Goodman (1962) gives the resulting shear stress as

$$q(\rho) = \frac{8\beta\rho}{\pi^2}\int_0^{\sqrt{1-\rho^2}} \frac{\ln x}{(1-x^2)^2}\,\mathrm{d}x. \tag{51}$$

This solution is not physical since near the contact edge, the shear stress will be larger than the normal pressure times the coefficient of friction. Although it is impossible to express the shear stress in closed form, this is possible for the surface stresses. The dimensionless radial stress due to the shear force becomes according to Hills *et al.* (1993)

$$\bar{\sigma}_{rr}^{q} = \frac{4\beta}{\pi}\left[\frac{2\rho}{3\pi}(2+\nu)-p+\frac{1-\nu}{3\rho^2}(1-p)\right], \quad \rho \leqslant 1 \tag{52}$$

$$\bar{\sigma}_{rr}^{q} = \frac{8\beta}{3\pi^2}\left[\frac{1-\nu}{\rho^2}\arctan\frac{1}{q}-(2+\nu)(q-\rho)-\frac{q}{\rho^2}[1-\nu+\rho^2(2+\nu)]\ln\frac{\rho}{q}\right], \quad \rho \geqslant 1. \tag{53}$$

2.4.3. *Complete slip.* If, instead, complete slip is assumed, no integral equation has to be formulated. The shear traction must be according to eqn (1)

$$q(\rho) = \mu p(\rho). \tag{54}$$

The radial stress can then be found by the methods applied above for the coupled problem. Johnson *et al.* (1973) gives the radial stress as

$$\bar{\sigma}_{rr}^{q} = \frac{16\mu}{\pi^2}\left[\frac{1-\nu}{\rho^2}\int_0^1 \frac{t^2\{K(t')-E(t')\}}{\sqrt{\rho^2-t^2}}\,dt+\int_0^1 \frac{t^2\{K(t')-E(t')\}}{(\rho^2-t^2)^{3/2}}\,dt\right], \quad \rho \geqslant 1. \tag{55}$$

The expressions above all make it possible to calculate the resulting stress distribution for an uncoupled problem by evaluating closed form expressions. The accuracy of the different methods will be discussed below.

3. INITIATION OF CONE CRACKS

The first visible damage arising during an indentation test in brittle materials (ceramics, glass etc.) is a ring crack emanating outside the contact perimeter normal to the surface. The radius of the crack is usually 5–40% larger than the contact radius. Upon further increase in load, this ring crack grows into the material at an inclined angle, away from the contact, and the familiar cone crack is formed. Later also radial cracks and crushing zones may develop (see Cook and Pharr, 1990 for discussion of crack types).

A fundamental assumption for the initiation of ring cracks is that the magnitude of the maximum principal stress is the governing parameter. For the frictionless contact and spherical indenters it is well known that the radial stress at the contact perimeter is the largest stress component. This implies that the stress distribution must differ from Hertz solution. In the presence of friction the distribution will change and therefore the location and magnitude of the largest principal stress will also change. For small values of the coefficient of friction the change in stress distribution will be small and concentrated around the contact region. The radial stress at the surface will still be the largest principal stress, the maximum will however be shifted outwards. The methods described above are utilized to calculate the resulting radial stress at the surface of the bodies for a given value of the coefficient of friction. The location of the maximum tensile principal stress is then taken as the point where the crack will be initiated.

4. MEASUREMENT OF THE COEFFICIENT OF FRICTION

The former analysis shows that the presence of friction is, at least qualitatively, the explanation for crack initiation outside the contact radius. For quantitative comparisons between the calculations and the experimental results the coefficient of friction also has to be experimentally measured. If the measured and the calculated coefficients of friction are equal, then it implies that friction is the cause of the observed crack radius increase.

The indenter materials were only available in the form of spheres (diameter 3 mm). In order to use these for the friction measurements, small steel blocks were manufactured (see Fig. 2). Three holes were drilled in to which the spheres were glued. The arrangement used

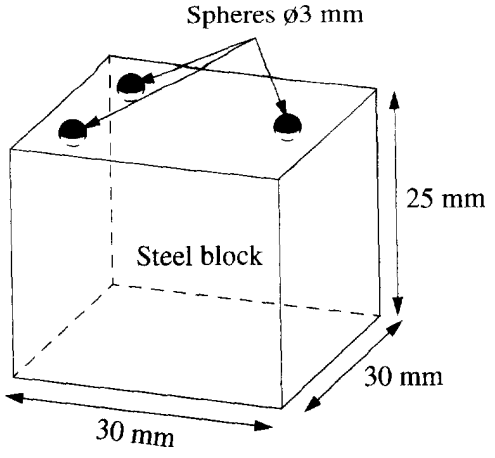

Fig. 2. Steel block used for measurement of the coefficient of friction.

for the experiments was a leaning plane. The leaning angle, α, of the plane was slowly increased until the entire steel block began to slide. This test method gives the static coefficient of friction. When solving the contact problem it is not fully clear if it is the static or the dynamic (sliding) coefficient of friction that should be used. The static coefficient determines when slip begins between the bodies but it will be another coefficient of friction that determines when the sliding will end (when the sliding velocity approaches zero). During the experiments it was observed that when the steel blocks had begun to slide they often continued with approximately constant velocity. Thus, the difference between the static and the dynamic coefficient of friction seems to be small for the material combinations under consideration.

From static equilibrium considerations of the steel block on the leaning plane, the coefficient of friction is obtained as

$$\mu = \tan \alpha, \tag{56}$$

where α is the leaning angle for which sliding begin.

The tests were performed using two different materials for the spheres (steel and WC) and several different ceramics and one glass. Both types of spheres are intended to be used as ball bearings and they are well polished. Approximate material properties are shown in Table 2 and the resulting coefficients of friction in Table 3. The values presented in Table 3 are the mean values from five tests. The scatter was for most material combinations around 5%. For the glass, however, the scatter was about 25%, which probably is due to small scratches on the surface of the samples. It was somewhat surprising that the coefficients

Table 2. Material properties

No.	Material	E/GPa	ν
1	$Al_2O_3+8\%ZrO_2$(SHM)	380	0.24
2	Al_2O_3(SHM)	380	0.24
3	$Al_2O_3+8\%ZrO_2$(IFÖ)	380	0.24
4	Al_2O_3(MM)	380	0.24
5	$Al_2O_3+15\%ZrO_2$(IBD-Rami)	380	0.24
6	$Al_2O_3+4\%SiO_2$(IFÖ)	380	0.24
7	SiC (Cercom)	455	0.17
8	TiB_2 (Cercom)	556	0.20
9	Sialon 2 (SHM)	400	0.20
10	Soda-lime glass	69	0.25
11	$Al_2O_3+25\%SiC_w$	330	0.22
12	SS142258 (Steel)	205	0.30
13	WC+8%Co	614	0.22

Table 3. Coefficients of friction

Material no.	Steel spheres E_c GPa	β	μ	WC spheres E_c GPa	β	μ
1	144.5	−0.061	0.320±0.017	248.1	0.072	0.150±0.008
2	144.5	−0.061	0.285±0.011	248.1	0.072	0.151±0.004
3	144.5	−0.061	0.380±0.024	248.1	0.072	0.275±0.029
4	144.5	−0.061	0.387±0.014	248.1	0.072	0.217±0.005
5	144.5	−0.061	0.418±0.006	248.1	0.072	0.253±0.017
6	144.5	−0.061	0.445±0.006	248.1	0.072	0.264±0.010
7	152.1	−0.064	0.289±0.032	271.4	0.079	0.215±0.007
8	162.2	−0.101	0.225±0.013	305.2	0.028	0.171±0.007
9	146.2	−0.054	0.426±0.014	253.2	0.087	0.230±0.005
10	55.5	0.181	0.207±0.054	66.1	0.262	0.130±0.009

of friction for the steel and WC spheres differed as much as Table 3 shows (often a factor 2). It is not possible to distinguish the two different spheres by visual inspection. The different values of μ for materials 1–6, which were all alumina based ceramics, indicate that it is not possible to obtain the coefficient of friction only from knowledge of which two materials are used. Materials 3, 6 and 9 had a rough surface, with clearly visible scratches from manufacturing, while all other materials had a smooth surface.

5. RESULTS

The results are here divided into three parts. First a parameter study is performed to clarify influence of the three parameters on the solution. Secondly the accuracy of the simpler uncoupled methods is examined. Finally, the calculated location of maximum tensile principal stress is compared with the radius of ring cracks found in experiments.

5.1. *Parametric studies*

As was found from the analysis in Section 2, the contact stress distribution will depend upon the difference in stiffness β and the coefficient of friction μ. It is often convenient to represent the solution as function of the slip radius. In Fig. 3 the relation between slip radius and the ratio μ/β is shown. Since the dependence on β is not very strong, only four different values have been used. As can be seen, eqn (46) is accurate even for $\beta = 0.2$, while for large values the difference becomes significant. In Fig. 4, the dimensionless load is shown. As is well known, friction hardly influences the load-displacement relation. The maximum increase is about 10%, but from Fig. 5 it is seen that the contact radius for the same case has decreased with 4%, which means that the increase of the physical load will be only about 5%. Thus, in practical indentation testing it is not possible to detect friction effects by monitoring the load and certainly not the contact radius.

The following figures concerns the change in stress distribution due to friction and in particular the location and magnitude of the maximum principal stress. For the stiffer body, the location of the maximum remains at the contact edge and as can be seen in Fig. 6, the magnitude increases. The amount of increase is a strong function of both β and c (or μ), the stress distribution is also dependent upon Poisson's ratio ν. Comparison of Figs 6a and b shows that an increase of ν from 0.15 to 0.35 approximately doubles the maximum stress for a given value of β. But since an increase of ν in the stiffer body also increases β the effect of varying Poisson's ratio will be even stronger. An interesting feature is that the solution for high values of c does not monotonically approach the value for complete stick ($c = 1$). The reason for this is that the complete stick solution is fundamentally different having $q(\rho) > \mu p(\rho)$ near the contact edge. This, of course, affects the stress at the contact edge.

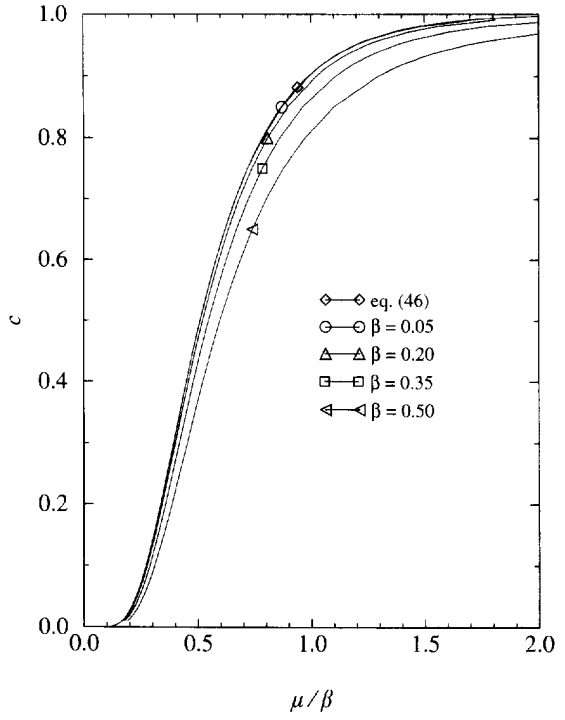

Fig. 3. Slip radius as function of μ/β.

For the softer body it is seen in Figs 7a and b that the magnitude of the maximum principal stress is instead decreasing with c, contrary to the results of the stiffer body. The variation of stress with the three parameters is as strong as for the stiffer body. There are, however, two differences. For the softer body an increase of ν will instead decrease the value of β and therefore the influence of ν will be less than that indicated by comparing Figs 7a and b. For the softer body the solution for high values of c monotonically approaches the complete stick value. This is because the maximum will occur outside the contact edge and therefore the exact distribution of the contact stresses will not be important. For both bodies the solution varies rapidly for small values of c. The implication of this is that even with a small coefficient of friction, Hertz solution gives a poor estimate of the maximum principal stress.

For the softer body the location of the maximum stress also changes. This is interesting for prediction of crack initiation. The dependence of the location on β, c and ν is shown in Figs 8a and b. Also for the location the dependence of all three variables is strong.

It is theoretically possible to change the magnitude of the maximum principal stress by a factor 10 (up or down) as well as moving the location of the maximum on the softer body to a radius of 2.5 times the contact radius. Thus, to analyse the stress distribution for an indentation test it is necessary to have accurate values of the constitutive parameters of both bodies as well as the coefficient of friction.

5.2. *Comparison of the different levels of approximation*

When comparing the coupled and the uncoupled analyses it is necessary to specify whether it is the indentation or the load that is given. For the case where the load and contact radius have the largest deviation from the Hertz solution (which is $\beta = 0.5$ and $c = 1$), $A \approx 1.088$ and $P^* \approx 0.7323$ giving the ratio between the scalings as

$$\frac{a/a_H|_P}{a/a_H|_\Delta} = \sqrt{A}\sqrt[3]{\frac{2}{3AP^*}} \approx 0.983. \tag{57}$$

It then follows that the dimensionless stresses for the coupled problem would be 1.7% less

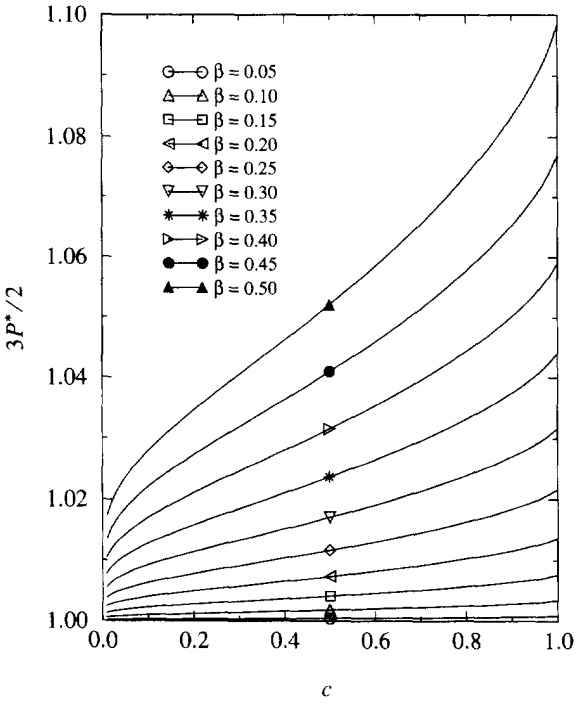

Fig. 4. Influence of friction on the dimensionless load.

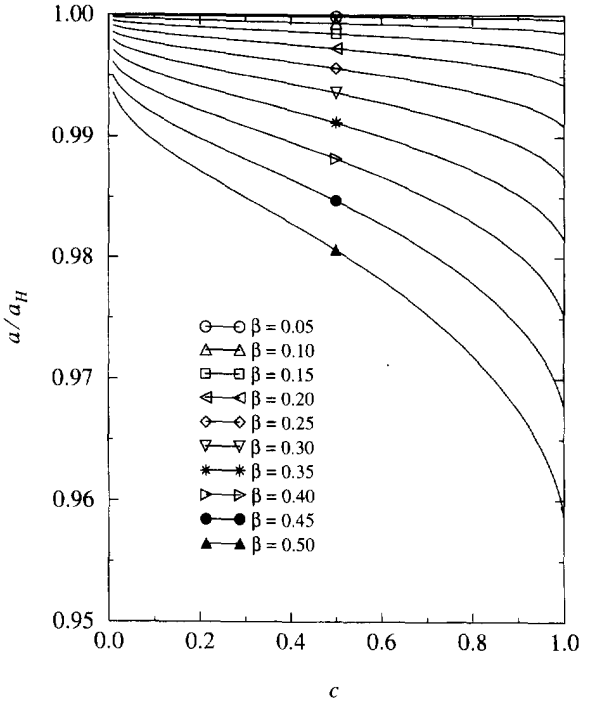

Fig. 5. Influence of friction on the contact radius.

than shown in the figures if the load instead was the controlled parameter. A corresponding shift in location of the stress point will occur according to the scaling introduced in eqn (33). This means that the difference between the scalings can be neglected with a good accuracy, which also holds for the prediction of the crack radius performed below. This means that the well known, closed form relations between load, indentation depth and contact radius known as Hertz solution can be used with very good accuracy except for extreme cases.

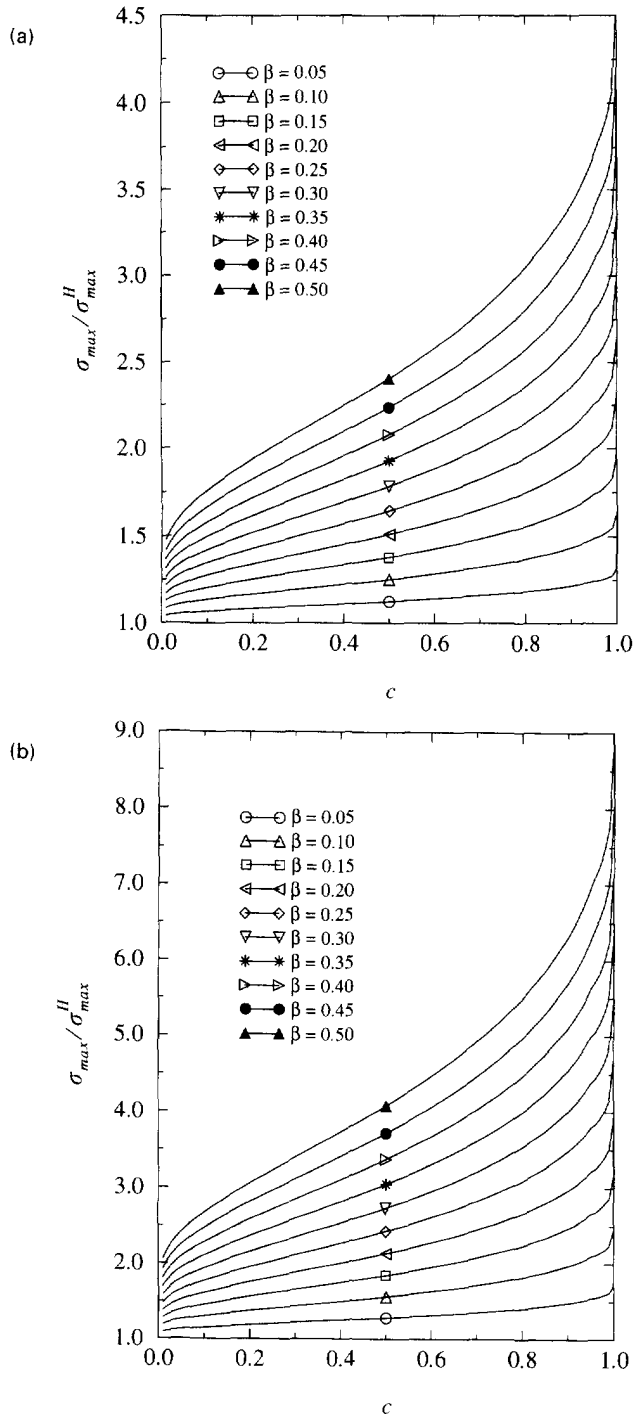

Fig. 6. (a) Ratio between maximum radial stress, with and without the influence of friction. The stiffer body ($v = 0.15$). (b) Ratio between maximum radial stress, with and without the influence of friction. The stiffer body ($v = 0.35$).

As pointed out earlier the use of an uncoupled analysis also simplifies the calculation of the stress distribution. Therefore it is of interest to examine the accuracy of these methods. Since it is the contact stress that will differ, it is only the variation of β and μ that is of interest. Calculations with different values of v have been performed, but since the difference between the methods does not change notably, only results for $v = 0.35$ are shown here. The methods are compared for different values of β. Since the complete stick solution is independent of μ they are shown as horizontal lines. For high values of the

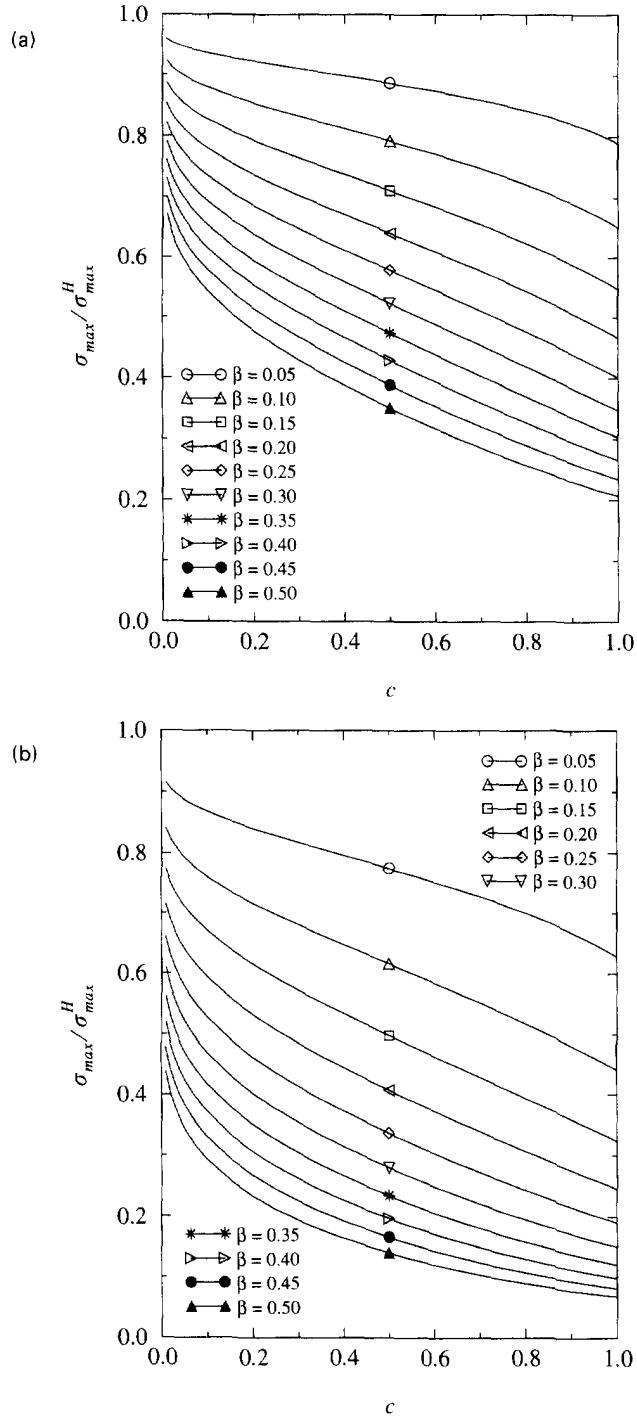

Fig. 7. (a) Ratio between maximum radial stress, with and without the influence of friction. The softer body ($\nu = 0.15$). (b) Ratio between maximum radial stress, with and without the influence of friction. The softer body ($\nu = 0.35$).

coefficient of friction the stick-slip solution approaches the complete stick solution. In Fig. 9, the maximum stress on the stiffer body is shown. The uncoupled stick-slip solution is very accurate. It is only for $\beta = 0.5$ and $\beta = 0.35$ at high values of the coefficient of friction that significant deviations occur. The complete stick solution is an upper bound for the uncoupled problem, but as can be seen especially for the higher values of β the stresses can be higher. For small values of β the complete stick solution is accurate for $\mu/\beta > 2$ which is of practical importance since $\mu \approx 0.2$ is a common value. The complete slip solution

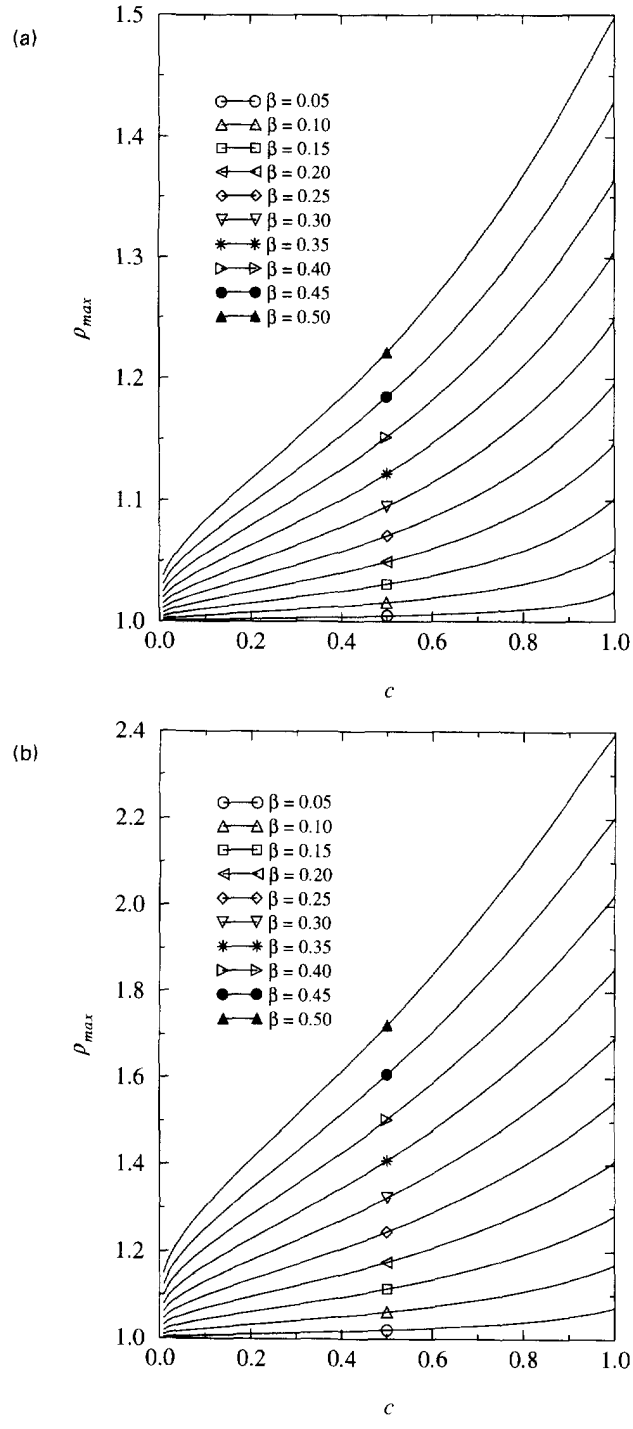

Fig. 8. (a) Location of the maximum radial stress on the softer body ($\nu = 0.15$). (b) Location of the maximum radial stress on the softer body ($\nu = 0.35$).

instead requires a low value of the coefficient of friction. Again for small values of β, this method is accurate if $\mu/\beta < 1$. Since both the complete slip and the stick-slip solution require numerical solution of integrals, the gain in using the complete slip solution is not worth the loss of accuracy.

In Fig. 10, the maximum stress on the softer body is shown and in Fig. 11 its location. The conclusions about the accuracy will be the same as for the stiffer body. The difference is that here the stresses are compared some distance away from the contact edge, which results in an even better agreement between the coupled and the uncoupled analysis.

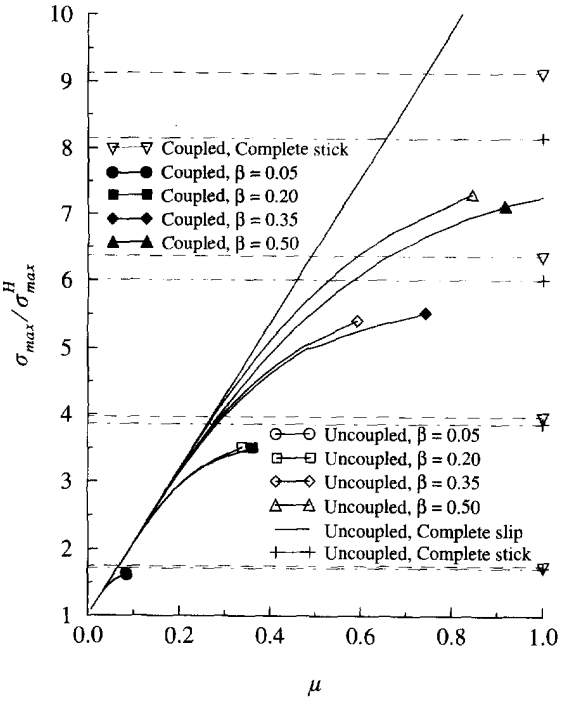

Fig. 9. Comparison of ratio between maximum radial stress, with and without the influence of friction for different levels of approximation. The stiffer body ($\nu = 0.35$).

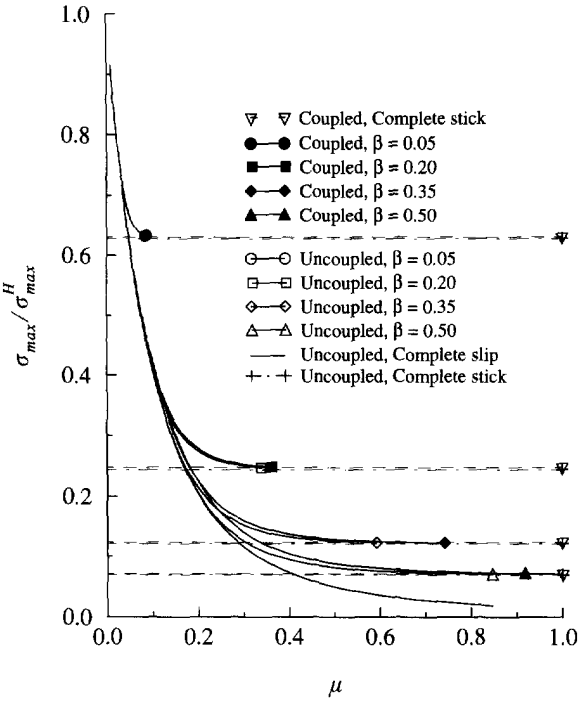

Fig. 10. Comparison of ratio between maximum radial stress, with and without the influence of friction for different levels of approximation. The softer body ($\nu = 0.35$).

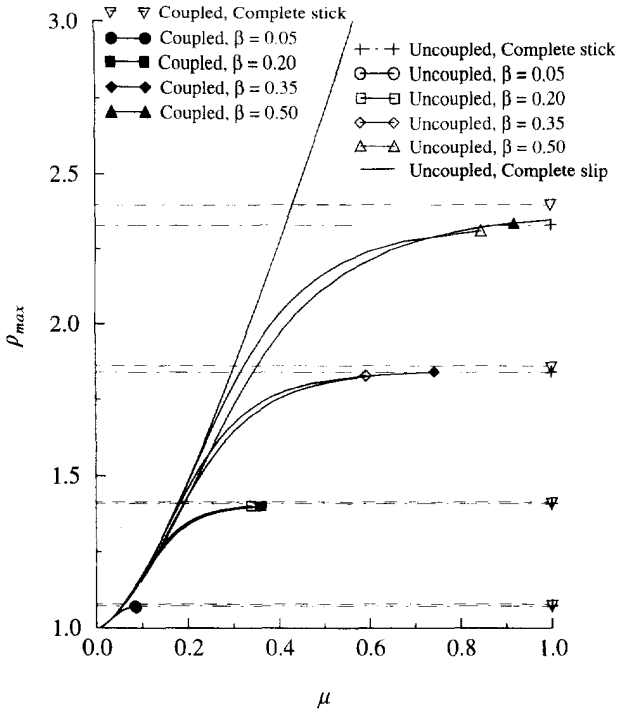

Fig. 11. Comparison of location of the maximum radial stress for different levels of approximation ($\nu = 0.35$).

5.3. *Comparison with experimental results*

In order to get a discriminating case for the solution method as well as for the assumptions made, some calculations were performed and compared with experiments. Results from Persson *et al.* (1992) were used, where steel spheres were indented into thick soda-lime glass plates (material no. 10 and 12 in Table 2). The ring cracks observed were approximately 29% larger than the theoretical contact radius. By applying a very thin layer of Au-Pd to the glass, the actual contact radius could be measured after removal of the load. It was shown that the theoretical and the actual contact radius were in excellent agreement, even for indentations giving a contact radius that was 30% of the sphere radius. In Fig. 12a, the contact shear stress distribution has been calculated for $\mu = 0.207$ which was the mean value for coefficient of friction obtained in the measurements. This gives $\mu/\beta = 1.14$ and, as can be seen, the uncoupled stick-slip and complete slip solutions are fairly accurate in the entire contact, while the complete slip solution, due to the large slip radius for this case, differs quite significantly except near the contact edge. Here also the pressure distribution from the coupled analysis multiplied with the coefficient of friction has been included. By comparing this curve with the complete slip curve it is seen that the contact pressure will be slightly underestimated in the centre of the contact and overestimated at the contact edge if the Hertz solution is utilized. In Fig. 12b, the corresponding distributions of radial stress are shown. The maximum stress will occur at a radius 16.6% larger than the contact radius predicted by Hertz solution. It is also seen that the uncoupled stick-slip solution is quite accurate and also the complete stick solution gives a fair agreement. The complete slip solution does not give good results in this case. Since the crack radius is underestimated a new calculation was performed with $\mu = 0.261$ (addition of the standard deviation) which is shown in Fig. 12c. Increasing the coefficient of friction increases the slip radius and therefore the complete stick solution will be more accurate for this case. But since the slip radius already was large in the previous calculation the coupled and the stick-slip solutions do not change much. The location of the maximum moves to a radius 18.2% larger than the contact radius. The complete slip solution will deviate even more and in this case it would predict a crack radius larger than the ones found in the experiments.

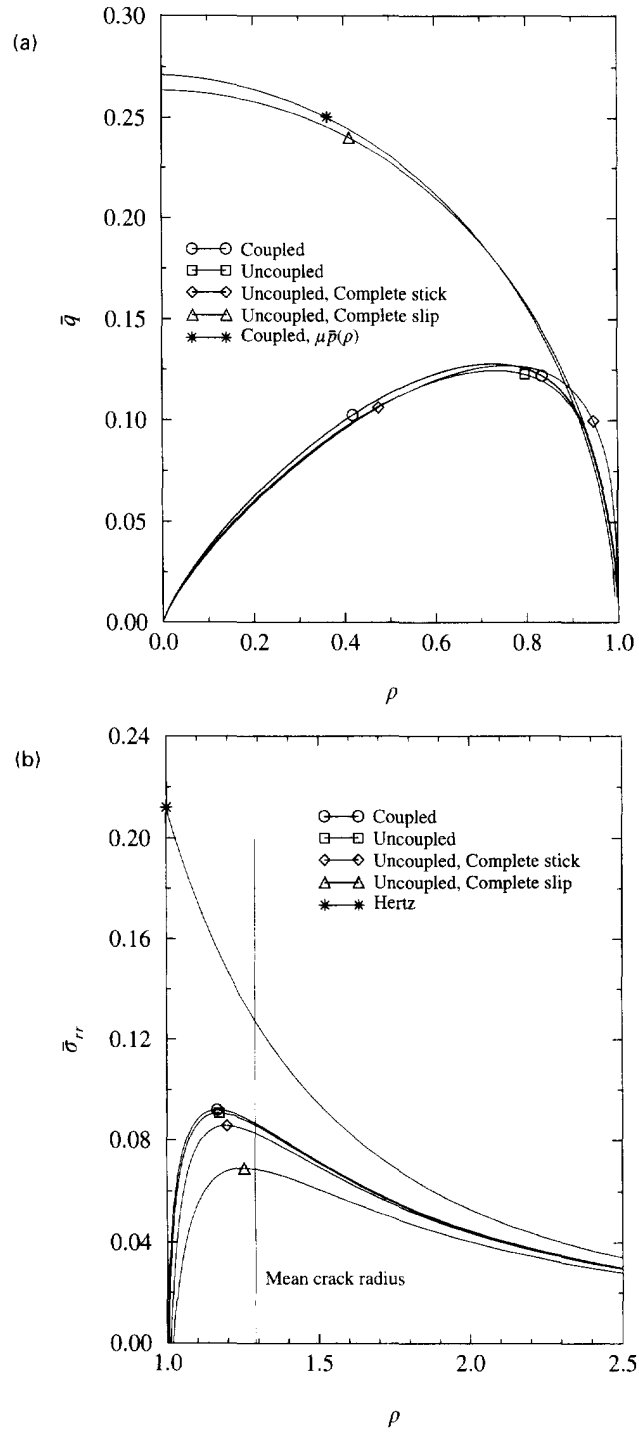

Fig. 12. (a) Contact shear stress calculated with different levels of approximation. Steel sphere indented into a glass block, $\mu = 0.207$. (b) Radial stress distribution calculated with different levels of approximation. Steel sphere indented into a glass block, $\mu = 0.207$. (c) Radial stress distribution calculated with different levels of approximation. Steel sphere indented into a glass block, $\mu = 0.261$.

(*Continued overleaf.*)

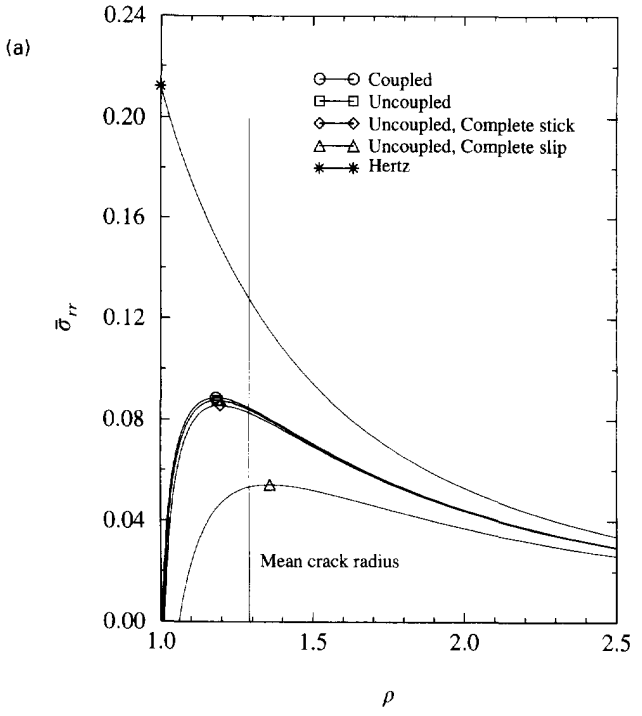

Fig. 12. *Continued.*

A similar comparison was made with experiments performed in Zeng *et al.* (1992a). Here alumina with 25% silicon carbide whiskers was indented by a wolfram carbide sphere. The material parameters are not reported, but in Zeng *et al.* (1992b) the Young's modulus has been found by indentation tests to be 330 GPa, which is somewhat low but will be used in the analysis. The Poisson's ratio of the composite is calculated according to the serial rule of mixture. The concentration of Al_2O_3 and SiC gives $\nu = 0.22$, which seems reasonable. Taking the elastic constants for the wolfram carbide from Table 2 gives the difference in stiffness $\beta = 0.108$.

This material was not available for measurement of the coefficient of friction. Looking at the different types of alumina in Table 3 show a quite large spread. Here $\mu = 0.25$ was chosen, which may be a bit on the high side. Results from the calculations are shown in Fig. 13. In this case $\mu/\beta = 2.31$ and therefore almost complete stick will occur. This results in an excellent agreement between all solutions except the complete slip. In Zeng *et al.* (1992a) the crack radius is reported to be 1.195 ± 0.041 times the contact radius. The calculated location of maximum principal stress is only 8.7% larger than the contact radius. Since complete stick already almost persists, an increase of the coefficient of friction will not change this result much.

6. CONCLUSIONS

Experimental studies have shown that ring cracks are formed during indentation of a sphere into a plate. If the plate material is brittle, the crack initiates at a location outside the contact region. The results of this paper show that friction between the two bodies plays a significant role in determining the location of the maximum principal tensile stress. It was also shown that the difference in stiffness between the bodies in contact, the coefficient of friction and the Poisson's ratio all three strongly influence the stress distribution in the surroundings of the contact. Furthermore, it was shown that an uncoupled analysis with a stick and a slip region will be sufficient for calculation of the radial stress distribution, except for values of β close to 0.5. In cases with low values of β and at least two times

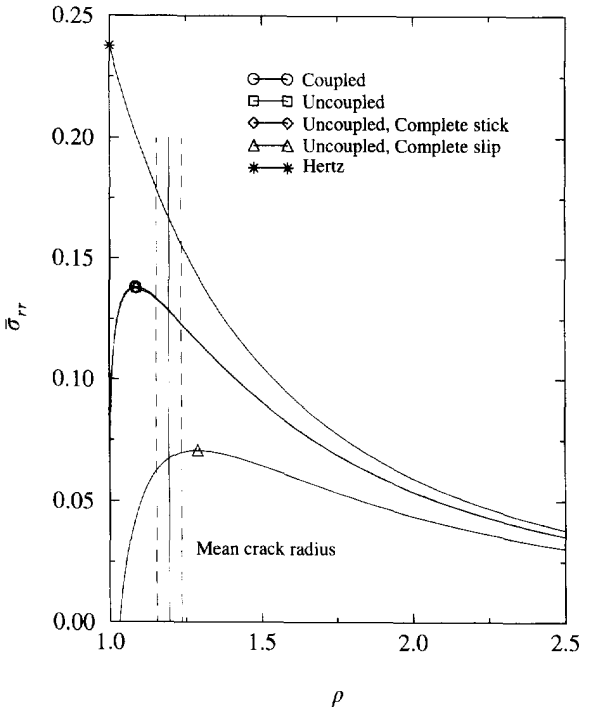

Fig. 13. Contact shear stress (hollow symbols) and radial stress distribution (filled symbols) calculated with different levels of approximation. Wolfram Carbide sphere indented into a whisker reinforced alumina block, $\mu = 0.261$.

higher value of the coefficient of friction, the closed form expression for the stress obtained from an uncoupled complete stick analysis can be used with good accuracy.

Since even a fairly small coefficients of friction produce large deviations from the Hertz solution it is not possible to neglect this effect if the stress distribution in the contact region is of interest. Due to the high pressure levels and quasi static conditions it will not be possible to significantly reduce the coefficient of friction by use of lubricants. The only way to avoid friction effects will be to use materials with the same elastic constants. This fact makes it doubtful to use indentation test for determination of material properties like the tensile strength. Using this method for fracture toughness testing will also give results that are affected by friction, especially for short ring cracks. For plastic properties, the circumstances are more favourable since the effective stress has its maximum below the surface (approximately half the contact radius). The friction induced stresses are self-equilibrating and hence the influence on stress distribution will decrease rapidly with increasing distance from the contact surface. However, if the difference in stiffness is large or if the plastic zone reaches the surface of the body, the effect of friction must be checked even for plasticity measurements.

Regarding frictional effects as an explanation for where cracks will occur, the conclusion is that friction gives a qualitative, but not a quantitative correct explanation. Since the contact pressure is very high when the crack initiates it is possible that Coulomb's law of friction no longer is valid. However in Johnson *et al.* (1973) the coefficient of friction is measured through torsion of a sphere under high axial load and since the conclusions from this work is the same as here, Coulomb's law should be valid. It is likely that a statistical distribution of strength also has to be considered, which has been done in for example Oh and Finnie (1967) and Hamilton and Rawson (1970). There however, the Hertz stress distribution without friction was used which will result in an strong overestimation of the spread in strength required to obtain an expected crack radius which agrees with the experimental findings. The three main conclusions drawn, can be summarized as

—the stress distribution in the contact area strongly depends on μ, β and ν;

—except for high values of β, the uncoupled analysis with a stick and a slip region gives accurate results;
—friction gives a qualitative, but not quantitative correct explanation for the phenomena that ring cracks develops outside the contact zone.

Acknowledgements—Thanks is directed to HB Utveckling AB for the financial support of this work and also to Mr Jonas Persson, Division of Ceramics, KTH, for providing the materials used in the friction measurements.

REFERENCES

Andersson, M. and Nilsson, F. (1995). A perturbation method used for static contact and low velocity impact. *Int. J. Impact Engng* **16,** 759–775.
Barber, J. R. (1983). The solution of elasticity problems for the half-space by the method of Green and Collins. *Appl. Sci. Res.* **40,** 135–157.
Chaudri, M. M. and Phillips, M. A. (1990). Quasi-static indentation cracking of thermally tempered soda-lime glass with spherical and Vickers indenters. *Phil. Mag. A.* **62,** 1.
Cook, R. F. and Pharr, G. M. (1990). Direct observation and analysis of indentation cracking in glasses and ceramics. *J. Am. Ceram. Soc.* **73,** 787–817.
Goodman, L. E. (1962). Contact stress analysis of normally loaded rough spheres. *J. Appl. Mech.* **29,** 515–522.
Green, A. E. and Zerna, W. (1968). *Theoretical Elasticity*, 2nd Ed., Oxford University Press, Oxford.
Greenwood, J. A. and Tripp, J. H. (1967). The elastic contact of rough spheres. *J. Appl. Mech.* **89,** 153–159.
Hamilton, B. and Rawson, H. (1970). The determination of the flaw distributions on various glass surfaces from Hertz fracture experiments. *J. Mech. Phys. Solids* **18,** 127–147.
Hills, D. A. and Sackfield, A. (1987). The stress field induced by normal contact between dissimilar spheres. *J. Appl. Mech.* **54,** 8–14.
Hills, D. A., Nowell, D. and Sackfield, A. (1993). *Mechanics of Elastic Contacts*, Butterworth-Heinemann Ltd.
Johnson, K. L., O'Connor, J. J. and Woodward, A. C. (1973). The effect of the indenter elasticity on the Hertzian fracture of brittle materials. *Proc. Roy. Soc. Lond.* **A334,** 95–117.
Johnson, K. L. (1985). *Contact Mechanics*, Cambridge University Press, Cambridge.
Lawn, B. R. and Wilshaw, T. R. (1975). *Fracture of Brittle Solids*, Cambridge University Press, Cambridge.
Lundberg G. and Sjövall, H. (1958). *Stress and Deformation in Elastic Contacts*, The Institution of Theory of Elasticity and Strength of Materials, Chalmers University of Technology, Gothenburg.
Mouginot, R. and Maugis, D. (1985). Fracture indentation beneath flat and spherical punches. *J. Mat. Sci.* **20,** 4354.
Noble, B. and Spence, D. A. (1971). Formulation of two-dimensional and axisymmetric problems for an elastic half-space. *Tech. Summary Report* 1089, Maths. Research Centre, University of Wisconsin.
Oh, H. L. and Finnie, I. (1967). The ring cracking of glass by spherical indenters. *J. Mech. Phys. Solids* **15,** 401–411.
Persson, J., Breder, K. and Rowcliffe, D. (1992). Loading rate effects during indentation and impact on glass with small spheres. *TRITA - MAC* - 0497, Materials Research Center, The Royal Institute of Technology (KTH).
Spence, D. A. (1968). Self similar solutions to adhesive contact problems with incremental loading. *Proc. Roy. Soc.* **A305,** 55–80.
Spence, D. A. (1973). An Eigenvalue problem for elastic contact with finite friction. *Proc. Camb. Phil. Soc.* **73,** 249–268.
Spence, D. A. (1975). The Hertz contact problem with finite friction. *J. Elasticity* **5,** 297–319.
Zeng, K., Breder, K. and Rowcliffe, D. (1992a). The Hertzian stress field and formation of cone cracks. Part II—determination of fracture toughness. *Acta Metall. Mat.* **40,** 2601–2605.
Zeng, K., Breder, K. Rowcliffe, D. and Herrström, C. (1992b). Elastic modulus determined by Hertzian indentation. *J. Mat. Sci.* **27,** 3789–3792.